

## Merging the gravity fields of the GRACE Follow-On Science Data System project using different weighting approaches

Artur Lenczuk\*, Anna Klos, Janusz Bogusz

Military University of Technology, Warsaw, Poland

e-mail: [artur.lenczuk@wat.edu.pl](mailto:artur.lenczuk@wat.edu.pl); ORCID: <http://orcid.org/0000-0002-9573-1302>

e-mail: [anna.klos@wat.edu.pl](mailto:anna.klos@wat.edu.pl); ORCID: <http://orcid.org/0000-0001-6742-8077>

e-mail: [janusz.bogusz@wat.edu.pl](mailto:janusz.bogusz@wat.edu.pl); ORCID: <http://orcid.org/0000-0002-0424-7022>

\*Corresponding author: Artur Lenczuk, e-mail: [artur.lenczuk@wat.edu.pl](mailto:artur.lenczuk@wat.edu.pl)

Received: 2023-03-13 / Accepted: 2023-06-01

**Abstract:** For over two decades, an essential information about global monthly gravity variations is provided by the GRACE mission and its successor, the GRACE Follow-On (GRACE-FO) mission. The temporal variations in gravity field from GRACE/GRACE-FO are determined based on the measurement of distance changes between two identical satellites using microwave ranging instruments. This process is carried out by various processing centers, which adopt different processing strategies and background models. This causes discrepancies in the resulting gravity fields. We address this problem by determining a monthly homogenous GRACE-FO gravity field solutions from June 2018 to November 2022 as provided by different processing centers included in the Science Data System (SDS) project, i.e. the Center for Space Research (CSR), the German Research Center for Geosciences (GFZ) and the Jet Propulsion Laboratory (JPL). We test three different weighting schemes. We show that for the last 4 years, at least 65% of continental areas are characterized by water decrease. We show that proposed merged solutions contain more signal information than individual ones based on the square root of the degree variance values. We note that the largest signal differences between individual and combined solutions occur for sectoral coefficients up to degree 40, and for zonal coefficients, the signal differences are twice as small. We also present that the differences in the spherical harmonic coefficients cause differences in global and local equivalent water height (EWH) changes. For example, the proposed merged solutions reduce root mean square scatter of EWH by 5–15% comparing to individual solutions.

**Keywords:** GRACE Follow-On, merged gravity field solution, variance component estimation, equivalent water height



The Author(s). 2023 Open Access. This article is distributed under the terms of the Creative Commons Attribution 4.0 International License (<http://creativecommons.org/licenses/by/4.0/>), which permits unrestricted use, distribution, and reproduction in any medium, provided you give appropriate credit to the original author(s) and the source, provide a link to the Creative Commons license, and indicate if changes were made.

## 1. Introduction

The Earth's gravity field changes according to subsurface and surface mass variations. Its temporal changes at a specific location are successfully measured using terrestrial gravimeters (Agnew et al., 2015). There are two types of gravimeters i.e., absolute and relative. The absolute gravimeters measure constant downward acceleration of gravity in absolute units ( $m/s^2$ ). The relative gravimeters measure gravity differences between the two locations. However, both instruments provide information about point-wise (local) characteristics of the gravity field changes.

The variations in the global gravity field are observed by the satellite gravimetric missions. To date, three gravimetric missions have been launched: (i) the Challenging Minisatellite Payload (CHAMP) (Reigber et al., 2002), (ii) the Gravity field and steady-state Ocean Circulation Explorer (GOCE) (Rummel, 2011) and (iii) Gravity Recovery and Climate Experiment (GRACE) (Tapley et al., 2004) with its successor GRACE Follow-On (GRACE-FO) (Landerer et al., 2020). They enable to determine the static part of Earth's gravity field (mean gravity field model) reflecting the physics of the Earth's interior or time-variable Earth's gravity field model reflecting the anomalous gravity signals with respect to a certain mean (Ince et al., 2019). The static gravity field models are computed based on data from satellite-based measurements, terrestrial gravity measurements and satellite-radar-altimetry-derived quantities. Undoubtedly, GRACE/GRACE-FO missions are fundamental in observing the global temporal gravity changes. Between 2002 and 2017 GRACE mission provided the continuous gravity field changes. After a nearly 1-year gap i.e., from July 2017 to May 2018, the GRACE-FO mission has been launched. Products of GRACE and GRACE-FO have spatial resolution of c.a. 300 km, which is a bit lower than the resolution of static gravity field model (Ince et al., 2019).

The estimation of gravity field from GRACE/GRACE-FO rely on precise measurements of the distance between twin spacecrafts, which is recalculated to the natural Earth's gravity field parameters (Tapley et al., 2004) at different processing centers. The process of gravity parameters estimation is complicated, and requires many sophisticated operations such as an inversion of distance between the twin GRACE/GRACE-FO spacecraft, application of different orbital parameters or non-gravitational corrections. Many parameter choices, various processing approaches or a range of available background models lead to discrepancies between gravity fields estimated during the processing of GRACE/GRACE-FO observations at different research centers, such as the Astronomical Institute of the University of Bern (AIUB, Switzerland) (Lasser et al., 2020), the Center for Space Research (CSR, Austin, U.S.) (Bettadpur, 2018), the German Research Center for Geosciences (GFZ, Potsdam) (Dahle et al., 2018), the Groupe de Recherche de Géodésie Spatiale (GRGS, France) (Lemoine et al., 2019), the Institute of Geodesy at the Graz University of Technology (ITSG, Austria) (Meyer-Gürr et al., 2018), the Jet Propulsion Laboratory (JPL, Maryland, U.S.) (Yuan, 2018), or the Tongji University (Tongji, China) (Chen et al., 2019). The above mentioned centers provide Level-0 (a raw data received twice per day from each satellite), Level-1 (the result of a non-destructive processing applied to the Level-0 data; data are processed using various corrections, parameter choices and solution strategies), Level-2 (the short term and static gravity field derived from

calibrated and validated GRACE/GRACE-FO Level-1 data; spherical harmonic form) or Level-3 (spherical harmonic coefficients transformed to gridded geopotential functions, e.g. gridded water equivalent mass values) products. The available products differ depending on processing centers causing discrepancies in the results, e.g. water storage changes, ocean mass changes or polar motion. So, it is difficult to note which data set should be chosen and which determined parameters credibly reflect real gravity changes.

To address this problem, researchers merged GRACE/GRACE-FO products from different processing centers which resulted in the so-called “averaged gravity field” and improved the quality of the gravity signal with regards to the individual solutions. For example, [Sasgen et al. \(2007\)](#) showed that in the merged solutions generated by an optimal Wiener filtering, the non-geophysical components (e.g. uncertainty in the accelerometer data) are better reduced than in the case of the four independent GRACE products provided by different processing centers. They showed better agreement with the predicted geoid height changes over Antarctica area for the merged solutions than for individual ones. For data provided by CSR, GFZ and JPL processing centers, [Sakumura et al. \(2014\)](#) developed an ensemble gravity field solution. They showed a significant noise reduction of the local relative water height variation over the oceans and river basins, e.g. the root mean square (RMS) error reduction by 5–10 mm for an arithmetic mean of GRACE solutions. [Jean et al. \(2018\)](#) tested five different combinations of spherical harmonic coefficients on the normal equation level ([Meyer et al., 2019](#)). They proposed the variance component estimation weighting schemes, which are also provided by the European Gravity Service for Improved Emergency Management (EGSIEM) project (<http://www.egsiem.eu>) and is applied to monthly GRACE/GRACE-FO gravity fields generated by the Combination Service for Time-variable Gravity Fields (COST-G; [Meyer et al., 2020](#)). They noticed that each combined solution is characterized by a lower noise compared to the individual contributions in both the spectral and the spatial domains. They showed that the signal strength for combined solutions is as good or better than individual solutions in 90% of analyzed months. They reduced non-seasonal variability by nearly 8% over the oceans and the RMS of differences between individual and combined solutions by up to 18% for Antarctic drainage basins.

In our research, we use data sets of spherical harmonic coefficients form provided by the official GRACE/GRACE-FO Science Data System (SDS, [Watkins et al., 2000](#)) centers i.e., CSR, GFZ and JPL. We focus on estimating new merged GRACE-FO solutions. The merged gravity field solutions are computed using weighting algorithms based on two different non-iterative schemes: coefficient-wise and field-wise, as well as two approaches of iterative variance component estimation. To assess the reliability of merged solutions, we compare them with mascon solution provided by the CSR and with data predicted using the WGHM hydrological model (WaterGAP Global Hydrological Model). The results we obtain help: (i) to indicate regions with extreme water changes observed for GRACE-FO period, (ii) to better understand the differences between individual gravity field solutions provided by processing centers and their combination, and (iii) to assess the coherence between individual and merged solutions. The results also emphasize the potential and advantages of merged solutions in comparison to individual solutions. We would like to notice that proposed weighting approaches are able to estimate merged

solutions based on different number and type of gravity field solutions provided by different processing centers. Also, authors expect that the presented approaches will give satisfying results for either GRACE or GRACE-FO solutions.

## 2. Data and methodology

We use the release 06 Level-2 spherical harmonic coefficients truncated up to degree and order 96 provided by three different SDS processing centers, i.e. CSR (Save, 2019), GFZ (Dahle et al., 2019) and JPL (Yuan, 2019) for the GRACE-FO period; each center is based on different background models used in processing of GRACE-FO observations (Dahle et al., 2019; Save, 2019; Yuan, 2019). We use 52 monthly data between June 2018 and November 2022. The presented results are in the form of the anomalies relative to GGM05C static gravity field model (Ries et al., 2016). Degree-1 coefficients are replaced following Sun et al. (2016), and degree-2 and degree-3 coefficients are replaced by Satellite Laser Ranging (SLR) estimates. All terms are implemented using Technical Note 14 (TN14). All corrections related to the low-degree terms are available at <https://podaac-tools.jpl.nasa.gov/drive/files/allData/gracefo>. Finally, the GRACE-FO north-south stripes are reduced using the isotropic Gaussian filter (Eq. 59 in Jekeli (1981)) with 300 km radii. Since we are performing a comparison of the results obtained from individual centers, rather than interpreting analyses, the Glacial Isostatic Adjustment (GIA) effect is not removed.

For the sake of comparison, we use also GRACE-FO data provided by the CSR in a mascon form (Save et al., 2016). We use release 06 of monthly TWS values on a grid of  $0.25^\circ$  per  $0.25^\circ$  within the range of  $89.875^\circ$ N/S for latitude and within the range of  $0.125^\circ$  to  $359.875^\circ$ E for longitude. More detailed information about the mascon processing can be found at <https://www.csr.utexas.edu/>. The TWS values predicted from WGHM model is also analyzed. We use a 2.2d version of the WGHM model (Schmied et al., 2021), which is developed at the University of Frankfurt and whose water changes are available from January 1901 to December 2019. We implement only months for the GRACE-FO period, i.e. since June 2018 until November 2022. TWS values predicted from WGHM are defined on a global grid of  $0.5^\circ$  per  $0.5^\circ$ , and provide information for 10 TWS compartments i.e., surface water, groundwater, soil moisture, snow water equivalent or irrigation. The TWS derived from GRACE-FO observations and predicted from WGHM are recalculated to spherical harmonic coefficients form using formulas included in Wahr et al. (1998). To estimate the merged GRACE-FO gravity field solutions from CSR, GFZ and JPL processing centers, we test various weighting schemes based on spherical harmonic coefficients. We propose algorithms using either non-iterative (Eq. (1) and Eq. (2)) or iterative (Eq. (3) and Eq. (4)) methods, for which the final merged solutions are calculated as a weighted mean of the CSR, GFZ and JPL solutions weighted by values estimated as follow:

- coefficient-wise (COEFF) weighting scheme:

$$w_{n,m}^{i,t} = \left[ \left( X_{n,m}^{i,t} - \bar{X}_{n,m}^t \right)^2 \right]^{-1} \quad (1)$$

– field-wise (FIELD) weighting scheme:

$$w_{n,m}^{i,t} = \left[ \frac{1}{N_{\text{coeff}}} \sum_{n=2}^{n_{\text{max}}} \sum_{m=0}^n \left( X_{n,m}^t - \bar{X}_{n,m}^t \right)^2 \right]^{-1} \quad (2)$$

– variance component estimation for coefficient-wise (VCE\_cw) weighting scheme:

$$w_{n,m}^{i,t,(k)} = \left[ \frac{\left( X_{n,m}^{i,t} - \bar{X}_{n,m}^t \right)^2}{\left( 1 - \frac{w_{n,m}^{i,t,(k-1)}}{\sum_{i=1}^{N_{\text{sol}}} w_{n,m}^{i,t,(k-1)}} \right)} \right]^{-1} \quad (3)$$

– variance component estimation for field-wise (VCE\_fw) weighting scheme:

$$w_{n,m}^{i,t,(k)} = \left[ \frac{\sum_{n=2}^{n_{\text{max}}} \sum_{m=0}^n \left( X_{n,m}^t - \hat{X}_{n,m}^{t,(k-1)} \right)^2}{N_{\text{coeff}} \left( 1 - \frac{w_{n,m}^{i,t,(k-1)}}{\sum_{i=1}^{N_{\text{sol}}} w_{n,m}^{i,t,(k-1)}} \right)} \right]^{-1} \quad (4)$$

where  $w$  means weights estimated for COEFF, FIELD, VCE\_cw and VCE\_fw schemes,  $i$  means index of time series of gravity field solution at month  $t$ ,  $k$  is a number of iteration.  $X_{n,m}$  reflects  $C_{nm}$  or  $S_{nm}$  spherical harmonic coefficients for  $n$  degree and  $m$  order,  $\bar{X}_{n,m}^t$  is arithmetic mean of CSR, GFZ and JPL spherical harmonic coefficients at month  $t$ .  $N_{\text{coeff}}$  and  $N_{\text{sol}}$  are number of spherical harmonic coefficients per gravity field (here  $N_{\text{coeff}}$  is equal to 4750) and number of used gravity field contributions (here  $N_{\text{sol}}$  is equal to 3), respectively.  $\hat{X}_{n,m}^{t,(k-1)}$  presents weighted mean of  $C_{nm}$  or  $S_{nm}$  spherical harmonic coefficients in  $k - 1$  iteration. In case of iterative approaches, the iteration process is stopped by analyzing the convergence of the Gauss-Newton method under a majorant condition (Ferreira et al., 2013). In our case, the convergence goes up to 5 iterations. Finally, the individual and merged spherical harmonic coefficients are used to estimate the equivalent water height (EWH) values using Eq. 1 in Ahi and Shuanggen (2019).

To estimate the variance of signal contained in each degree of the spherical harmonic coefficients, the square root of degree variance is calculated (Sakumura, 2014) following the formula:

$$\sigma_n^2 = \frac{1}{M} \sum_{j=1}^M \sum_{m=0}^n C_{nm}^{*2}(t_j) + S_{nm}^{*2}(t_j) \quad (5)$$

where  $j$  means the selected month of GRACE-FO data and  $M$  is a total number of all chosen months, the  $C_{nm}^*$  or  $S_{nm}^*$  mean spherical harmonic coefficients for individual and merged GRACE-FO solutions.

### 3. Results and discussion

Firstly, we study global TWS changes to assess the agreement between GRACE-FO solutions provided by individual processing centers belonging to SDS project. We use least-squares estimation to derive the values of trends and annual amplitudes of TWS changes (Fig. 1). We see that the majority of areas are characterized with water storage decrease. We obtain negative trend on 65% of land areas. The extreme negative trend (smaller than  $-2$  cm/yr) is observed for the southern part of North America, the western and southern parts of South America, and the eastern part of Asia. The areas selected for both Americas are characterized with progression from wet to dry period causing water decrease already during the last years of GRACE and GRACE-FO period. For the Asia regions, the precipitation increasing is observed (Hong et al., 2022). This has also been noticed for last years of GRACE (Rodell et al., 2018). The minimum trend near  $-12$  cm/yr is observed for Greenland, where the extreme ice mass losses are reported. Since mid-2018, ice decline around of 300 billion metric tons per year was noticed, with a record near  $532 \pm 58$  billion metric tons between September 2018 and August 2019 (Moon et al., 2020). Negative trend of TWS changes in North America is caused by dry conditions (decreasing rainfall and high temperatures). According to the U.S. Drought Monitor map more than 50% of the U.S. areas are characterized with at least severe drought conditions during the last years. The significant negative trend smaller than  $-3$  cm/yr in South America reflect water decrease, which is caused by reduced precipitation. The decline in precipitation is affected by, among other things, the positive sea surface temperature anomalies for ocean areas, sudden stratospheric warming phenomenon, heating in the stratosphere and troposphere, as well as El Niño effects (Gomes et al., 2021). The strong effect of a warming climate on TWS trend values is also captured for the Caspian Sea

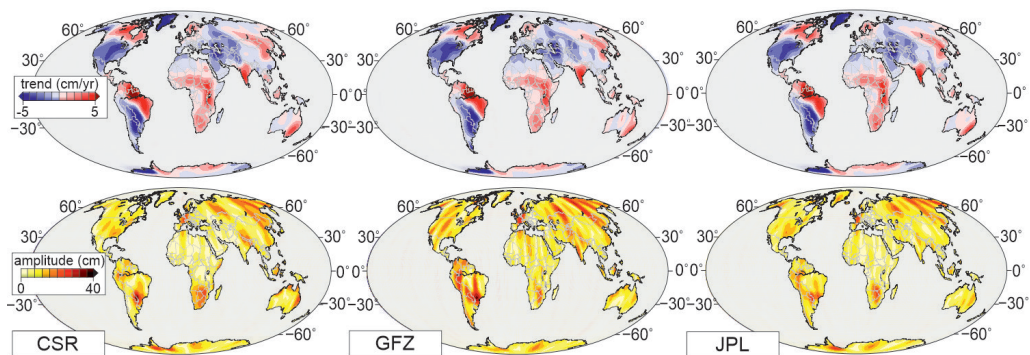


Fig. 1. The linear trend (top row) and annual amplitude (bottom row) of GRACE-FO TWS values obtained from spherical harmonic coefficients provided by the CSR (left column), GFZ (middle column) and JPL (right column) processing centers for the period between June 2018 and November 2022

region, where a continuous surface water decline is noticed; the Caspian Sea' surface area shrink by 23% for 9 m and by 34% for 18 m drop of sea level in this century (Prange et al., 2020). We obtain the extreme positive trend for GRACE-FO in the northern part of North America, the eastern part of South America, the central and southern parts of Africa, India, the eastern part of Asia and southern part of Australia region. We get maximum trend over +7 cm/yr for the northern Amazon area, where increase in precipitation is observed for the last years (Espinoza et al., 2022). The water storage changes in Africa are climate-related. We note the spatial coherency between regions characterized by positive trend and areas where heavy rains and floods occur (CRED, 2019). According to data provided by the World Meteorological Organization, India and eastern Asia regions are affected by systematically increasing and excessive monsoon rains, which reflect the obtained positive TWS trend. The southeastern Australia is affected by disastrous bushfires, exacerbated by anthropogenic climate change (van Oldenborgh et al., 2021), for which we obtain TWS trend near 2-3 cm/yr. It is related with low temperatures and high rainfall associated with La Niña conditions (Copernicus Climate Change Service). In general, the spatial distribution of TWS trend estimated for GRACE-FO period coincides as well with trend values distribution estimated for GRACE period (Rodell et al., 2018). Only the central part of North America (High Plains Aquifers), the southeastern part of Brazil and its surroundings or Beijing surrounding are characterized by the opposite TWS trend, which reflects the progression from dry/wet to wet/dry conditions. In case of amplitude of annual oscillation (Fig. 1, bottom row), the spatial distribution of the extreme values do not overlap with values estimated from GRACE or GRACE/GRACE-FO, for which the maximum values are mainly observed around the equator (Save et al., 2016). For GRACE-FO solutions, we obtain values of annual amplitude above 20 mm for southern Brazil (due to systematic rainfall anomaly; Nascimento et al., 2020), southern Africa (flooded area touched by variable rainfall severity; McBride et al., 2020), western Europe (groundwater variations; Tegel et al., 2020) and northern Asia (rising temperatures intermingled with monsoons; Ciavarella et al., 2021; Grigorieva and Livenets, 2022). The greatest annual amplitude equal to 40 mm is observed in southern Brazil. Moreover in case of CSR and JPL solutions, amplitudes over 10 mm are observed in the southern U.S. and Bangladesh surroundings. For the GFZ solution, we also get significant amplitudes over 25 mm in the western part of the Amazon river basin; CSR and JPL solutions show twice smaller annual amplitude. Due to location in the equatorial areas, they are contributed mainly by large impact of surface water resources on river basins, which is caused by heavy precipitation (Espinoza et al., 2016; Ouyang, et al., 2020).

Analyzing the maps presented in Figure 1, we notice that TWS values determined from individual GRACE-FO solutions are characterized by a similar spatial pattern of trend and annual amplitude in a global sense. However, values differ significantly on a regional scale, depending on the processing center.

Taking the above differences into consideration, we suggest to determine the homogeneous GRACE-FO monthly gravity field solutions. To do that, we use a weighted mean of three individual solutions and four different weighting schemes described by equations (1)–(4) in Section 2. The averaged weights of spherical harmonic coefficients obtained for CSR, GFZ and JPL solutions are presented in Figure 2 up to degree and order 96.

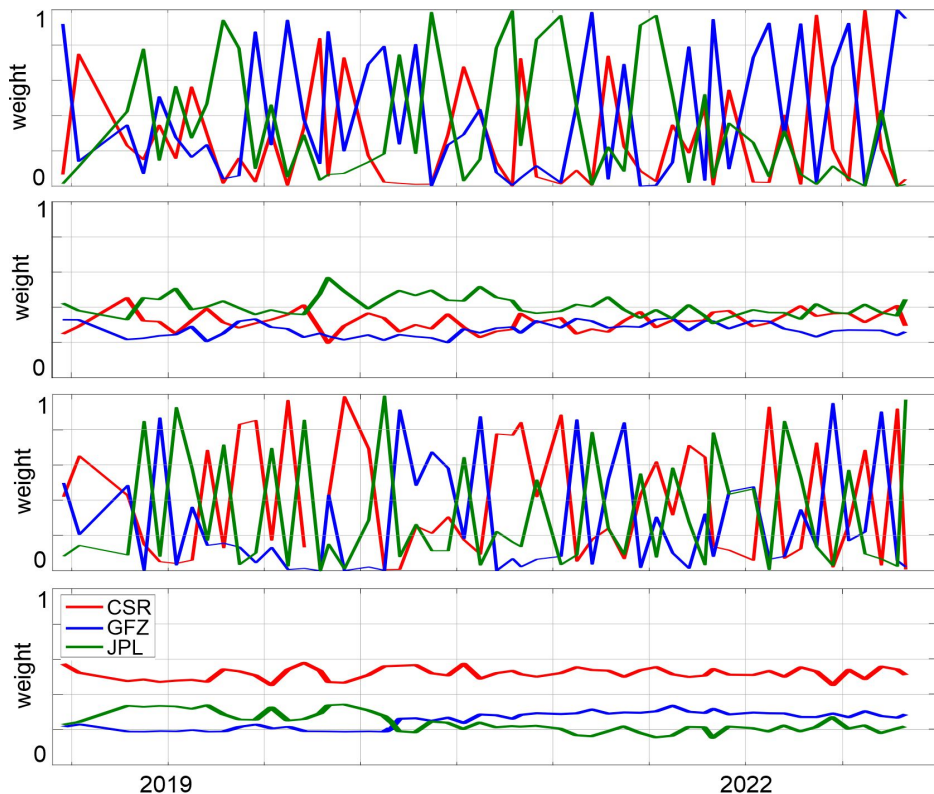


Fig. 2. Monthly normalized averaged weights derived by coefficient-wise (first row), field-wise (second row), and variance component estimation for coefficient-wise scheme (third row) and for field-wise scheme (fourth row) of GRACE-FO spherical harmonic coefficients. For each month, the weights are estimated as average values of all  $C_{nm}$  and  $S_{nm}$  coefficients up to degree and order 96

The magnitudes of weights estimated for three individual solutions differ each other (Fig. 2). The largest monthly variations are noted for the coefficient-wise (COEFF) scheme (first row) with the greatest differences appearing for the period 2020–2021. The lowest magnitudes of weights are obtained for the CSR individual solution (red curve). For the field-wise (FIELD) scheme (second row), weights are similar for all individual solutions, which means that in this scheme the weighted mean of individual solutions will be close to the arithmetic mean. In the case of variance component estimation for coefficient-wise scheme (VCE\_cw) (third row), the obtained weights are similar to COEFF solution; we notice monthly variations of weights for all individual solutions. However, for VCE\_cw we obtain more months with the largest CSR weights compared to COEFF variant. For variance component estimation for field-wise scheme (VCE\_fw) (fourth row), the CSR solution will have the greatest impact on the merged solution. The magnitudes of weights obtained for CSR solution are 2–3 times larger than the magnitudes of weights estimated for the GFZ (blue curve) and JPL (green curve) solutions. Magnitudes of weights are comparable for the entire period. It should only be noted that since 2021, the magnitudes

of weights estimated for the GFZ solution are larger than the magnitudes of weights estimated for the JPL solution; weights increase and decrease for both solutions. Figure 2 shows that the individual spherical harmonic coefficients have different impact on the merged solution, according to various weighting schemes.

To assess the quality of the four generated merged solutions, we compare them with external dataset and analyze the strength of the signal and information contained in each of them. Firstly, we analyze the values of square root of the degree variance of spherical harmonic coefficients (Fig. 3) for the individual, merged and mascon GRACE-FO solutions; mascon solution is applied here as a reference. Moreover, the results are compared with the degree variance of spherical harmonic coefficients predicted from WGHM hydrological model. The results we obtain reveal overall compliance between different solutions. All individual solutions provide similar large-scale (global) hydrological signals (Fig. 1), but small-scale (local) signals are different due to the discrepancies in the square root of the degree variance for coefficients for degrees higher than 30. For presented individual (dashed curves) and weighting (solid curves) solutions, we notice decreasing signal values with an increasing degree; it is coherent with the expected pattern of the degree amplitude curves of the models for the geophysical processes, such as hydrological models (orange solid curve). Similar changes are also observed for individual solutions (dashed curves). The values of degree variance estimated for the GFZ solution are the most similar to the WGHM values, especially for degrees up to 80. It should be noted that the values of

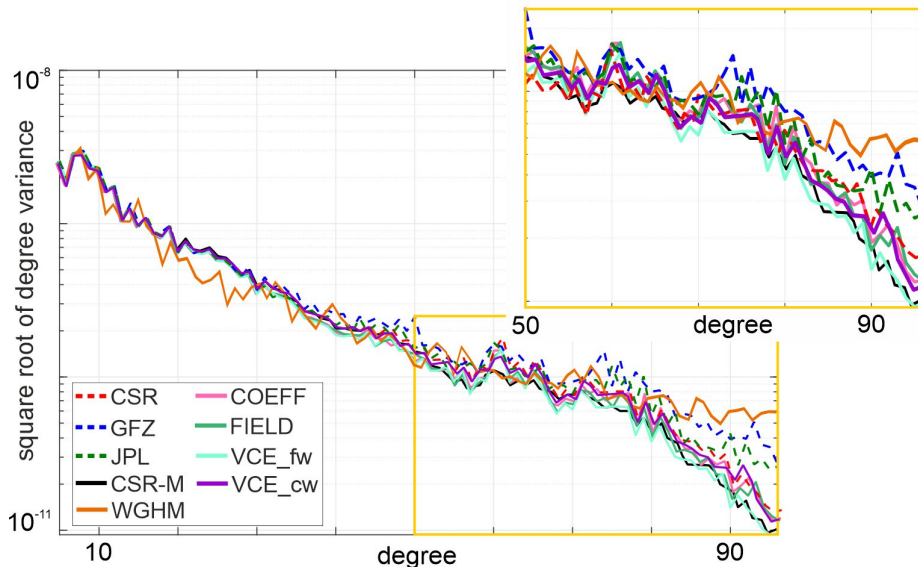


Fig. 3. Scatter of square root of the degree variance (unitless) of spherical harmonic coefficients values for degrees up to 96 estimated for GRACE-FO weighting approaches: coefficient-wise (COEFF), field-wise (FIELD), variance component estimation for field-wise scheme (VCE\_fw), variance component estimation for coefficient-wise scheme (VCE\_cw) (solid curves), and for spherical harmonic coefficients provided by GRACE-FO processing centers: CSR, GFZ, JPL (dashed curves). We also add spherical harmonic coefficients estimated for GRACE-FO CSR-provided mascon solution (CSR-M, black solid curve) and the WGHM hydrological model (orange solid curve)

degree variance for WGHM differ from the values estimated for the GRACE-FO mascon solution because WGHM does not contain data for Greenland, Antarctica and oceans. The decrease in root mean square variance of individual GRACE-FO solutions between degree 10 and 20 may be related to filter and degree dependency (Han et al., 2005). Also, signal differences are observed above 30 degrees for all solutions and around 45–50 for individual ones, which reflect probably the prominent north-south stripes in gravity fields (Svehla, 2018). The similar patterns have already been noticed by Lenczuk et al. (2020) for various GRACE solutions. But it is not observable for GRACE-FO mascon solution derived by the CSR (black solid curve). Moreover, we also note that root mean square values estimated for the GFZ solution differ the most from the other solutions. It has been already presented by Chen et al. (2021) for monthly RMS calculated for EWH changes in global oceans mass or by Abe et al. (2012) for gravity variations compared to superconducting gravimeters. For individual GRACE-FO solutions, the greatest amount of information is obtained for the CSR solution (red dashed curve), for which features similar variances to COEFF and FIELD (pink and green solid curves). The merged solution obtained with the VCE\_fw scheme is the most similar to the CSR-provided mascon solution (black solid curve in Fig. 3); this is especially evident for spherical harmonic coefficients up to degree 80. Individual GRACE-FO solution from the CSR is the most similar to all merged solutions, especially to the one obtained with the VCE\_cw scheme. We notice that VCE\_cw contains less signal than VCE\_fw, mainly for degrees up to 80. The presented values of degree variance agree well with a slight reduction of geoid degree power of various gravity field models at 60–150 degrees for GRACE/GRACE-FO mascons, and combined hydrological and oceanic models (Chen et al., 2020). The results also agree well with mean of monthly signal for atmosphere, ocean, ice or solid earth mass variation fields (Gruber et al., 2011) for both merged and individual solutions.

Secondly, we analyze the amount of information contained in each individual and merged solutions. We assess the amount of signal information contained in spherical harmonic coefficients for each gravity field solutions in comparison to VCE\_fw solution (adopted as the reference), which contains the greatest variance of signal (Fig. 3). The differences between VCE\_fw, and other merged and individual solutions are presented in Figure 4. The largest amount of information for coefficient differences are contained up to degree and order 40 of spherical harmonic coefficients for merged solutions and the individual CSR solution, and up to degree and order 60 for the individual GFZ and JPL solutions. CSR solution is more consistent with merged solutions than other individual solutions. The greatest signal differences between VCE\_fw and other solutions occur for sectoral coefficients, and also for tesseral coefficients for the GFZ and JPL solutions. The presented results are similar to those obtained by Sakumura et al. (2014). They noted the strongest correlation between weighted and individual GRACE time-variable gravity field solutions for zonal coefficients, for which we obtain the smallest differences. The largest signal differences are included mainly up to degree 10 for all solutions. The differences are twice as small for sectoral coefficients. It should be noted that obtained coefficient discrepancies may also represent the noise still contained in the GRACE fields after smoothing north-south stripes; here they are removed by Gaussian filter. Much less information is contained for all data sets for degree up to 60 (Fig. 3) than for low-term

spherical harmonic coefficients. Consequently, the differences presented in Figure 4 for high-term spherical harmonic coefficients are also two/three times smaller than for low-term ones. In case of the both variance component estimation solutions (VCE\_fw and VCE\_cw), the signal is almost identical. The signal difference is slight; signal is at least 10 times smaller than for individual and other merged solutions. So due to the high similarity in degree variance for both variance component estimation solutions (Fig. 3) and values of spherical harmonic coefficients (not presented here) we adopt only three (namely, COEFF, FIELD, VCE\_fw) weighting schemes for further analysis.

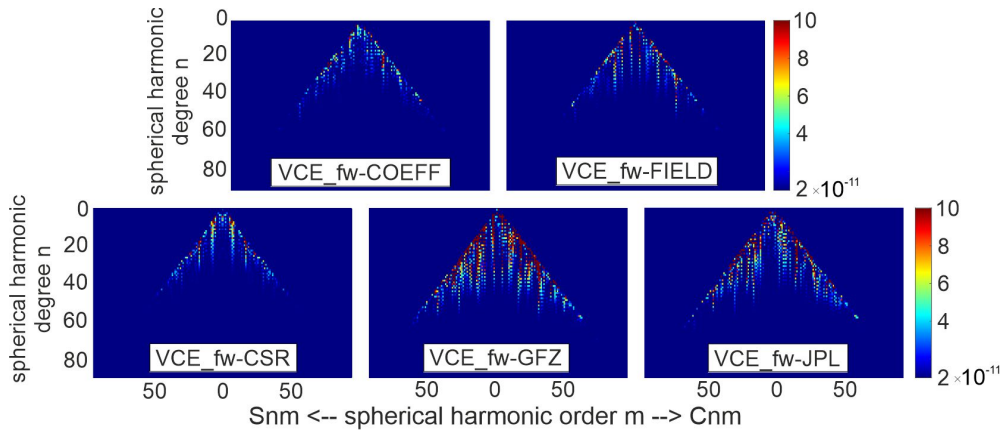


Fig. 4. Differences of spherical harmonics between variance component estimation for field-wise scheme (VCE\_fw) and coefficient-wise (COEFF) or field-wise (FIELD) schemes are presented in top row. Differences between VCE\_fw scheme and the CSR, GFZ and JPL individual solutions are presented in bottom row

Thirdly, we analyze the differences of global TWS changes estimated from merged and individual solutions. To assess the differences between them, we estimate the RMS values for the individual solutions (i.e. CSR, GFZ, JPL) and differences between individual solutions and the three merged solutions obtained with COEFF, FIELD and VCE\_fw weighting schemes. The spatial distribution of extreme RMS values and their magnitude are almost identical for all individual solutions (Fig. 5, first row). In case of continental areas, the largest RMS discrepancies are observed for: Alaska, Greenland, Hudson Bay surroundings, Scandinavia, which are affected by strong glacial isostatic adjustment and African Great Lakes, Caspian Sea, Amazon, Indus river basins areas, which are characterized with high surface water changes (Getirana et al., 2017). For these areas we obtain RMS values greater than 25 cm for all individual solutions (Fig. 5). In case of ocean areas, we also observe similarities between all individual solutions. The largest RMS diversity near 15 cm occur mainly in North America, Greenland surrounding and in south hemisphere areas, which are related to ENSO effects (Muis et al., 2018). We obtain the mean EWH RMS values near 14.5 cm for all individual solutions. The obtained extreme RMS values are comparable to extreme RMS values estimated for GRACE mission data and climate models (Jensen et al., 2020). RMS values we get for the differences between individual solutions and merged solutions show that the proposed merged solutions

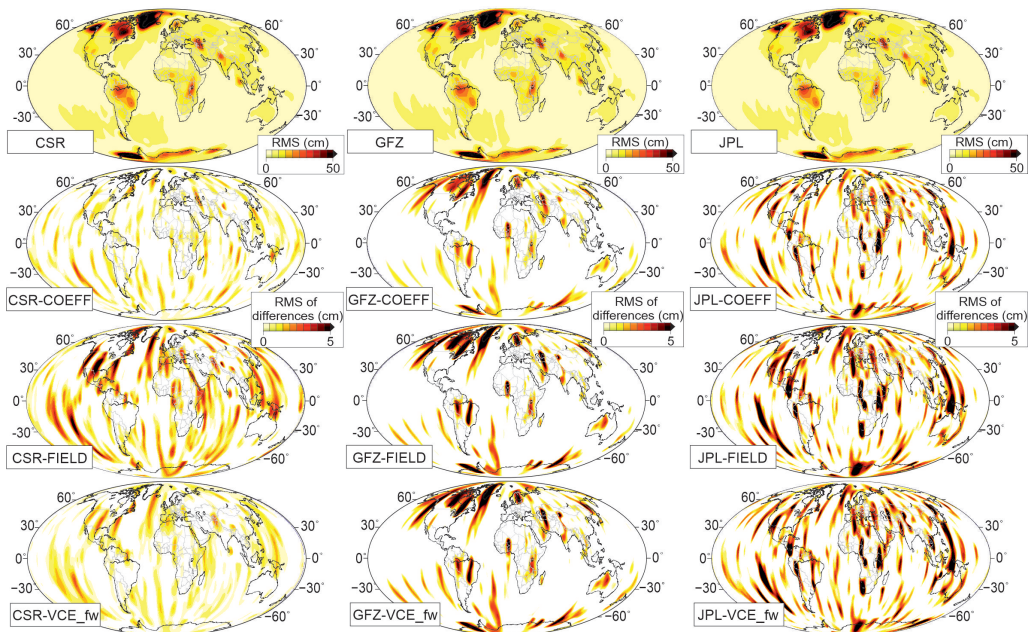


Fig. 5. The RMS of EWH values estimated for individual CSR, GFZ, JPL solutions (first row) and for the differences between individual solutions and merged solutions (from second to fourth rows) for coefficient-wise (COEFF), field-wise (FIELD) and variance component estimation for field-wise (VCE\_fw) schemes. Values are given in cm

reduce the RMS by 5–15% compared to individual ones (Fig. 5, from second to fourth rows). The spatial distribution of RMS of the differences estimated between the individual solutions and merged solutions is similar for all weighting schemes we use, but magnitude of them are significantly different. We get mean values of c.a. 1.5 cm for COEFF and over 2 cm for FIELD and VCE\_fw for GFZ and JPL; for CSR the values are several times smaller. It is worth noticing that the spatial distribution of extreme RMS of the differences is related to north-south stripes present in the GRACE-FO solution for both continental and ocean areas. This highlights that proposed merged solutions eliminate signal noise more efficiently than individual ones. For all cases, the largest differences occur mainly for equatorial areas and for regions located in high latitudes of the northern hemisphere; these regions do not coincide with regions characterized with the greatest RMS values. For CSR individual solution we obtain the smallest RMS of the differences compare to merged solutions; the GFZ individual solution is characterized with the largest values. The largest RMS of the differences is obtained for the FIELD weighting scheme for all individual solutions (Fig. 5). For all cases, we get values larger than 5 cm for North America and central Asia. For GFZ one, there are also maximum values near Greenland, Hudson Bay surroundings, Scandinavia, which are related with glacial isostatic adjustment effect and near Antarctica, which are related with variations in glacier mass. The most marked north-south stripes are observed for RMS of the differences computed versus JPL. We note nearly the identical differences for all merged solutions. Comparing the individual

solutions to merged ones, we obtain the smallest RMS of the differences for CSR and COEFF, and CSR and VCE\_fw. The values are less than 1 cm, excluding Caspian Sea and Tibet. For the VCE\_cw scheme, the RMS of the differences are similar to VCE\_fw results for all individual solutions; we do not present the results here.

Moreover, we analyze the local changes of EWH for areas characterized with extreme trend and/or annual amplitude presented in Figure 1. We select four regions, i.e., (i) Amazon river basin (with trend greater than 5 cm/yr), (ii) Zambezi river basin (with trend greater than 3 cm/yr), Murray–Darling river basin (with annual amplitude greater than 25 mm and trend greater than 3 cm/yr) and Loire river basin (with annual amplitude greater than 30 mm). Regional study shows a good agreement of monthly EWH values between individual and merged solutions. Figure 6 presents the results for merged solutions. We obtain the extreme EWH differences up to 15% between individual and merged solutions or between various merged solutions. The smallest differences of monthly EWH variations between all merged solutions are obtained for Amazon river basin (first row in Fig. 6), which is characterized with strong annual water changes. The decline in EWH in last months of 2019 reflects Amazon wildfires, which is caused by extreme drought conditions (Yuan et al., 2022). For the next months, the positive trend is affected by

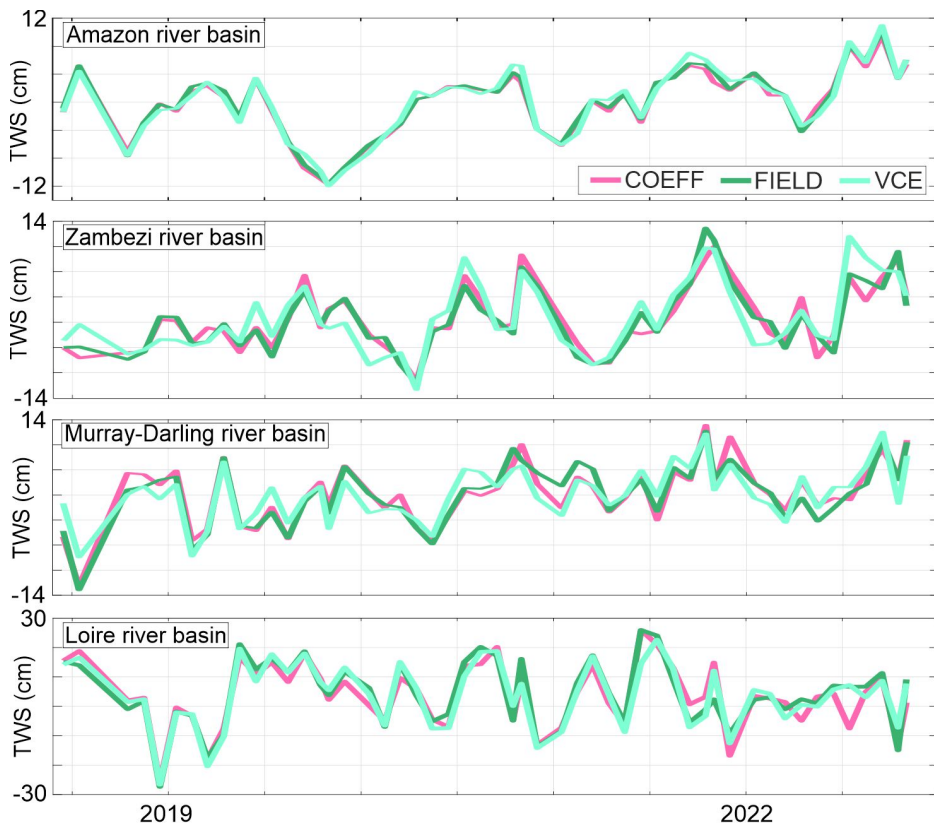


Fig. 6. Time series of EWH changes estimated for Amazon (first row), Zambezi (second row), Murray–Darling (third row) and Loire (fourth row) river basins estimated from merged SDS GRACE-FO solutions

progression from dry to wet conditions ended by strong flood in mid-2022. Zambezi river basin is also characterized with temporally coherent changes in EWH for all merged solutions (second row in Fig. 6). The largest discrepancies occur in autumn and winter periods every year (mainly from July to December). The intermittent dry (temperature rise) and wet (heavy rains) periods are captured by GRACE-FO in the analyzed period, for which changes in last months are affected by increased precipitation (Chisanga et al., 2022). For Australian region, the largest discrepancies between the merged solutions are noted in the first (mid-2018 to 2019), mid-term (mid-2020 to mid-2021) and last (after 2022) months of GRACE-FO period, which are related to dry and wet periods for the Murray–Darling river basin region. EWH variations in 2018–2019 and 2020–2021 show rainfall deficiencies and a large-scale natural flooding event (Higgs et al., 2022), respectively. In case of European area (Loire river basin), we obtain over twice greater seasonal changes (near 20 mm) than for other regions (bottom row in Fig. 6). We also notice EWH decline caused by temperature rise in 2019 and 2021 (Ribes et al., 2022), which is recharge not enough by rainfall. Consequently, the water storage is decreasing and water resources depend on groundwater in this region (Petersen-Perlman et al., 2022).

Finally, we analyze the statistic of monthly EWH values (Table 1), and linear trend and annual amplitude of EWH values (Table 2) estimated for the differences between individual and merged solutions. Table 1 shows that the EWH values we obtain for individual and merged solutions are similar (Table 1). EWH mean and median values are close to 0 mm. However, there are differences in the extreme (minimum and maximum) EWH values estimated between individual and merged solutions. We obtain the differences in the range of  $\pm 1$  cm to  $\pm 7$  cm; the largest discrepancies are observed for GFZ for all merged solutions. They mainly overlap with regions characterized with maximum values of TWS annual amplitude, i.e. southern parts of Brazil, Africa and Asia or western part of Europe (Fig. 1, bottom row). For these regions, we also determine the largest discrepancies of annual amplitude calculated between individual and merged solutions (Table 2). We obtain extreme values of the differences up to  $\pm 2$  mm. The mean values are near 1 mm; median values are similar. In case of trend parameter, the values of the differences are close to 0 mm/yr. However, we get maximum and minimum values of trend up to 12 mm/yr, which occur in Greenland, the southern part of North America, the western part of South America and India areas; there are cover with regions characterized with extreme TWS trend values (Fig. 1, top row).

Table 1. The averaged statistics of monthly EWH values [mm] estimated for the differences between individual solutions and merged solutions

	CSR–	GFZ–	JPL–	CSR–	GFZ–	JPL–	CSR–	GFZ–	JPL–
	COEFF			FIELD			VCE_fw		
min	–21.1	–75.6	–47.3	–29.0	–57.7	–54.5	–11.9	–76.1	–56.1
max	20.9	78.6	48.0	–29.0	59.8	55.2	12.2	79.2	57.7
mean	0.0	0.0	–0.1	0.0	0.0	–0.1	0.0	0.0	–0.1
median	0.0	0.1	–0.2	0.0	0.2	–0.2	0.0	0.2	–0.3

Table 2. The statistics of linear trend and annual amplitude [mm] of EWH values estimated for the differences between individual solutions and merged solutions

		CSR-	GFZ-	JPL-	CSR-	GFZ-	JPL-	CSR-	GFZ-	JPL-
		COEFF			FIELD			VCE_fw		
trend	min	-2.9	-11.5	-6.1	-3.7	-9.1	-6.4	-1.9	-11.9	-7.1
	max	2.8	11.6	6.8	3.5	9.0	7.5	2.2	11.8	8.3
	mean	0.0	-0.1	0.0	0.0	-0.1	0.0	0.0	-0.1	0.0
	median	0.0	0.0	-0.1	0.0	0.0	-0.1	0.0	0.0	-0.1
annual amplitude	min	-6.0	-16.3	-14.4	-6.4	-14.5	-14.0	-3.0	-19.2	-18.2
	max	11.5	19.4	13.5	6.1	16.9	16.2	4.6	20.5	15.5
	mean	0.7	1.6	0.4	0.5	1.4	0.2	0.2	1.1	-0.1
	median	0.6	1.4	0.4	0.4	1.2	0.4	0.2	0.9	0.1

#### 4. Summary

In the following research, we present and analyze the differences between monthly GRACE-FO gravity field solutions provided by processing centers included in the SDS project, i.e. CSR, GFZ and JPL centers, in a form of spherical harmonics. We determine and compare global trend and annual amplitude of TWS changes. We note that for the last 4 years, most land areas (over 65%) are characterized with water decreasing with values less than  $-10$  cm/yr reflecting a decrease of ice masses in Greenland. The maximum trend over  $7$  cm/yr is estimated for the northern Amazon, for which precipitation increasing is observed during last years. We notice that maximum values of GRACE-FO TWS annual amplitude do not occur mainly near equatorial regions as for GRACE TWS. For TWS changes recorded by the GRACE-FO, extreme seasonal changes are observed for the southern Brazil, southern Africa, western Europe and northern Asia regions. In case of linear trend, we obtain better agreement between all individual solutions than for annual amplitude.

We also focus on demonstrating the advantages of the merged gravity field solutions compared to individual ones. To determine a monthly homogenous GRACE-FO gravity field solutions, we propose four different weighting schemes: coefficient-wise, field-wise and two types of variance component estimation. We show that the individual solutions have different impact on merged solutions according to various weighting schemes. For example, (i) for COEFF solution, each individual solution has a significant impact to final merged solution in different months, (ii) the weights estimated for FIELD solution are similar for each solutions during entire period, (iii) for VCE\_cw and VCE\_fw solutions the weights are mainly dominant by the CSR individual solution. It is noticed by values of the square root of the degree variance, for which weights estimated from CSR individual solution are the most comparable to merged solutions. Then, we assess the spherical harmonic signal differences determined between VCE\_fw and other solutions. The results show that more information is contained within merged solutions than within individual

ones. It is also emphasized by the best similarity between the values of square root of the degree variance estimated for merged and mascon solutions. We also obtain the highest signal differences between merged and individual solutions up to degree 40 for sectorial spherical harmonic coefficients. We get twice smaller values for zonal coefficients than for sectorial coefficients.

The differences we obtain for spherical harmonic coefficients cause variations in global EWH changes estimated from various solutions. We note that the proposed merged solutions reduce RMS scatter of EWH changes by 5–15% compare to individual solutions. RMS of EWH differences are related with GRACE-FO north-south stripes. It emphasizes that merged solutions eliminate signal noise more efficiently than individual ones. The maximum values of RMS of differences even up to 5 cm are obtained for FIELD scheme comparing to all individual solutions. They occur mainly for equatorial areas and for regions located in high latitudes of the northern hemisphere; the spatial patterns of differences do not overlap with RMS values. Comparing all individual solutions to merged solutions, the smallest RMS of the differences are obtained for CSR, especially CSR and COEFF or CSR and VCE\_fw. For the VCE\_cw, the RMS of the differences are similar to VCE\_fw results for all individual solutions.

Finally, we analyze the local EWH changes estimated from merged solutions for four selected regions i.e., Amazon, Zambezi, Murray–Darling and Loire river basins. We show good agreement for monthly EWH series between various merged solutions. The results we obtain reflect well extreme event periods such as drought in 2019 for Amazon caused by wildfire, in 2018/2019 for Murray–Darling area reflecting rainfall deficiencies or temperature rise for Loire river basin in 2019 and 2021. There are also many flood events, e.g. in mid-2022 for Amazon reflecting progression from dry to wet conditions, in 2022 for Zambezi region caused by rainfall increasing or in 2020/2021 for Murray–Darling basin induced by large-scale natural flooding event.

Our results show that there are still EWH differences in short-term and extreme event periods between series determined for individual and merged solutions. We obtain the extreme values of EWH differences calculated between individual and merged solutions of less/more than  $\pm 7$  cm. Also, we notice the significant discrepancies of linear trend and annual amplitude of EWH values estimated for the differences between individual solutions and merged solutions. We show the differences up to  $\pm 12$  mm/yr and  $\pm 20$  mm for linear trend and annual amplitude, respectively. Thus, the reader should be aware that the magnitude of EWH changes for local study may be affected by selection of individual solutions. It is noticeably visible for regions characterized with extreme values of trend, annual amplitude and RMS.

### Author contributions

Conceptualization: A.L.; data collection and curation: A.L.; methodology: A.L.; visualization: A.L., A.K., J.B.; writing – original draft: A.L.; writing – review & editing: A.L., A.K., J.B.; supervision: A.K., J.B.

## Data availability statement

CSR, GFZ and JPL data in a form of spherical harmonic coefficients solution are available on: <http://icgem.gfz-potsdam.de/series> website. CSR mascon solution are available on: [http://www2.csr.utexas.edu/grace/RL06\\_mascons.html](http://www2.csr.utexas.edu/grace/RL06_mascons.html) website. WGHM hydrological model has been provided by the University of Frankfurt after personal contact, doi: <https://doi.org/10.5194/hess-18-3511-2014>.

## Acknowledgements

This study is financed by National Science Centre, Poland (NCN), grant number 2021/N/ST10/01472.

## References

- Abe, M., Kroner, C., Förste, C. et al. (2012). A comparison of GRACE-derived temporal gravity variations with observations of six European superconducting gravimeters. *Geophys. J. Int.*, 191(2), 545–556. DOI: [10.1111/j.1365-246x.2012.05641.x](https://doi.org/10.1111/j.1365-246x.2012.05641.x).
- Ahi, G.O., and Shuanggen, J. (2019). Hydrologic mass changes and their implications in mediterranean-climate Turkey from GRACE measurements. *Remote Sensing*, 11(2), 120. DOI: [10.3390/rs11020120](https://doi.org/10.3390/rs11020120).
- Agnew, D.C., Alfe, D., Allen, R.M. et al. (2015). *Treatise on Geophysics (Second Edition)*. ScienceDirect: Elsevier.
- Bettadpur, S. (2018). GRACE 327-742 (CSR-GR-12-xx) (Gravity Recovery and Climate Experiment), UTCSR Level-2 Processing Standards Document (Rev. 5.0, April 18, 2018), (For Level-2 Product Release 0006), Center for Space Research, The University of Texas at Austin.
- Chen, Q., Shen, Y., Chen, W. et al. (2019). An optimized short-arc approach: methodology and application to develop refined time series of Tongji-Grace2018 GRACE monthly solutions. *J. Geophys. Res. Solid Earth*, 124(6), 6010–6038. DOI: [10.1029/2018jb016596](https://doi.org/10.1029/2018jb016596).
- Chen, Q., Shen, Y., Kusche, J. et al. (2020). High-resolution GRACE monthly spherical harmonic solutions. *J. Geophys. Res. Solid Earth*, 126(1), e2019JB018892. DOI: [10.1029/2019jb018892](https://doi.org/10.1029/2019jb018892).
- Chen, J., Tapley, B., Tamisiea, M.E. et al. (2021). Error assessment of GRACE and GRACE Follow-On mass change. *J. Geophys. Res. Solid Earth*, 126(9), e2021JB022124. DOI: [10.1029/2021JB022124](https://doi.org/10.1029/2021JB022124).
- Chisanga, Ch.B., Mubanga, K.H., Sichigabula, H. et al. (2022). Modelling climatic trends for the Zambezi and Orange River Basins: implications on water security. *Water Clim. Change*, 13(3), 1275–1296. DOI: [10.2166/wcc.2022.308](https://doi.org/10.2166/wcc.2022.308).
- Ciavarella, A., Cotterill, D., Stott, P. et al. (2021). Prolonged Siberian heat of 2020 almost impossible without human influence. *Clim. Change*, 166, 9. DOI: [10.1007/s10584-021-03052-w](https://doi.org/10.1007/s10584-021-03052-w).
- CRED (2019). Disasters in Africa: 20 Year Review (2000–2019). Cred Crunch Newsletter, Issue No. 56.
- Dahle, C., Flechtner, F., Murböck, M. et al. (2018). GRACE 327-743 (Gravity Recovery and Climate Experiment), GFZ Level-2 Processing Standards Document for Level-2 Product Release 06 (Rev. 1.0, October 26, 2018), (Scientific Technical Report STR – Data; 18/04), Potsdam: GFZ German Research Centre for Geosciences. DOI: [10.2312/GFZ.b103-18048](https://doi.org/10.2312/GFZ.b103-18048).
- Dahle, C., Flechtner, F., Murböck, M. et al. (2019). GRACE-FO D-103919 (Gravity Recovery and Climate Experiment Follow-On), GFZ Level-2 Processing Standards Document for Level-2 Product Release 06 (Rev. 1.0, June 3, 2019), (Scientific Technical Report STR – Data; 19/09), Potsdam: GFZ German Research Centre for Geosciences. DOI: [10.2312/GFZ.b103-19098](https://doi.org/10.2312/GFZ.b103-19098).

- Espinoza, J.C., Segura, H., Ronchaili, J. et al. (2016). Evolution of wet-day and dry-day frequency in the western Amazon basin: Relationship with atmospheric circulation and impacts on vegetation. *Water Resour. Res.*, 52, 11, 8546–8560. DOI: [10.1002/2016WR019305](https://doi.org/10.1002/2016WR019305).
- Espinoza, J.-C., Marengo, J.A., Schongart, J. et al. (2022). The new historical flood of 2021 in the Amazon River compared to major floods of the 21st century: Atmospheric features in the context of the intensification of floods. *Weather Clim. Extremes*, 100406. DOI: [10.1016/j.wace.2021.100406](https://doi.org/10.1016/j.wace.2021.100406).
- Ferreira, O.P., Gonçalves, M.L.N. and Oliveira, P.R. (2013). Convergence of the Gauss–Newton method for convex composite optimization under a majorant condition. *SIAM J. Optim.*, 23(3), 1757–1783. DOI: [10.48550/arXiv.1107.3796](https://doi.org/10.48550/arXiv.1107.3796).
- Getirana, A., Kumar, S., Giroto, M. et al. (2017). Rivers and floodplains as key components of global terrestrial water storage variability. *Geophys. Res. Lett.*, 44, 10359–10368. DOI: [10.1002/2017GL074684](https://doi.org/10.1002/2017GL074684).
- Gomes, M.S., de Albuquerque Cavalcanti, I.F., and Müller, G.V. (2021). 2019/2020 drought impacts on South America and atmospheric and oceanic influences. *Weather Clim. Extremes*, 100404. DOI: [10.1016/j.wace.2021.100404](https://doi.org/10.1016/j.wace.2021.100404).
- Grigorieva, E.A., and Livenets, A.S. (2022). Risks to the Health of Russian Population from Floods and Droughts in 2010–2020: A Scoping Review. *Clim.*, 10(3), 37. DOI: [10.3390/cli10030037](https://doi.org/10.3390/cli10030037).
- Gruber, T., Bamber, J.L., Bierkens, M.F.P. et al. (2011). Simulation of the time-variable gravity field by means of coupled geophysical models. *Earth Sys. Sci. Data Discussions*, 4(1), 27–70. DOI: [10.5194/essd-4-27-2011](https://doi.org/10.5194/essd-4-27-2011).
- Han, S.-C., Shum, C.K., Jekeli, C. et al. (2005). Non-isotropic filtering of GRACE temporal gravity for geophysical signal enhancement. *Geophys. J. Int.*, 163(1), 18–25. DOI: [10.1111/j.1365-246X.2005.02756.x](https://doi.org/10.1111/j.1365-246X.2005.02756.x).
- Higginson, W., Cobb, A., Tschierchke, A. et al. (2022). The Role of Environmental Water and Reedbed Condition on the Response of Phragmites australis Reedbeds to Flooding. *Remote Sens.*, 14(8), 1868. DOI: [10.3390/rs14081868](https://doi.org/10.3390/rs14081868).
- Hong, H., Sun, J., and Wang, H. (2022). Interannual Variations in Summer Extreme Precipitation Frequency over Northern Asia and Related Atmospheric Circulation Patterns. *J. Hydrometeor.*, 23(4), 619–636. DOI: [10.1175/JHM-D-21-0177.1](https://doi.org/10.1175/JHM-D-21-0177.1).
- Ince, E.S., Barthelmes, F., Reißland, S. et al. (2019). ICGEM -15 years of successful collection and distribution of global gravitational models, associated services and future plans. *Earth Syst. Sci. Data*, 11, 647–674. DOI: [10.5194/essd-11-647-2019](https://doi.org/10.5194/essd-11-647-2019).
- Jean, Y., Meyer, U., and Jäggi, A. (2018). Combination of GRACE monthly gravity field solutions from different processing strategies. *J. Geod.*, 92, 1313–1328. DOI: [10.1007/s00190-018-1123-5](https://doi.org/10.1007/s00190-018-1123-5).
- Jensen, L., Eicker, A., Dobslaw, H. et al. (2020). Emerging Changes in Terrestrial Water Storage Variability as a Target for Future Satellite Gravity Missions. *Remote Sens.*, 12(23), 3898. DOI: [10.3390/rs12233898](https://doi.org/10.3390/rs12233898).
- Jekeli, C. (1981). Alternative methods to smooth the Earth's gravity field. *Tech. Rep.*, 327, Department of Geodetic Science and Surveying, Ohio State Univ., Columbus, OH.
- Landerer, F.W., Flechtner, F.M., Save, H. et al. (2020). Extending the Global Mass Change Data Record: GRACE Follow-On Instrument and Science Data Performance. *Geophys. Res. Lett.*, 47, e2020GL088306. DOI: [10.1029/2020GL088306](https://doi.org/10.1029/2020GL088306).
- Lasser, M., Meyer, U., Arnold, D. et al. (2020). AIUB-GRACE-FO-operational – Operational GRACE Follow-On monthly gravity field solutions. DOI: [10.5880/ICGEM.2020.001](https://doi.org/10.5880/ICGEM.2020.001).
- Lemoine, J-M, Biancale, R., Reinquin, F. et al. (2019). CNES/GRGS RL04 Earth gravity field models, from GRACE and SLR data. DOI: [10.5880/ICGEM.2019.010](https://doi.org/10.5880/ICGEM.2019.010).
- Lenczuk, A., Leszczuk, G., Klos, A. et al. (2020). Comparing variance of signal contained in the most recent GRACE solutions. *Geod. Cartogr.*, 69(1), 19–37. DOI: [10.24425/gac.2020.131084](https://doi.org/10.24425/gac.2020.131084).

- Meyer, U., Jean, Y., Kvas, A. et al. (2019). Combination of GRACE monthly gravity fields on the normal equation level. *J. Geod.*, 93, 1645–1658. DOI: [10.1007/s00190-019-01274-6](https://doi.org/10.1007/s00190-019-01274-6).
- Meyer, U., Lasser, M., Jaeggi, A. et al. (2020). International Combination Service for Time-variable Gravity Fields (COST-G) Monthly GRACE-FO Series. V. 01. GFZ Data Services. DOI: [10.5880/ICGEM.COST-G.002](https://doi.org/10.5880/ICGEM.COST-G.002).
- Meyer-Gürr, T., Behzadpur, S., Ellmer, M. et al. (2018). ITSG-Grace2018 – Monthly, Daily and Static Gravity Field Solutions from GRACE. DOI: [10.5880/ICGEM.2018.003](https://doi.org/10.5880/ICGEM.2018.003).
- McBride, Ch.M., Kruger, A.C., and Dyson, L. (2020). Changes in extreme daily rainfall characteristics in South Africa: 1921–2020. *Weather Clim. Extremes*, 38, 1000517. DOI: [10.1016/j.wace.2022.100517](https://doi.org/10.1016/j.wace.2022.100517).
- Moon, T.A., Tedesco, M., Box, J.E. et al. (2020). Greenland Ice Sheet. Arctic Report Card: Update for 2020. Retrieved February 2023 from <https://arctic.noaa.gov/Report-Card/Report-Card-2020/ArtMID/7975/ArticleID/901/Greenland-Ice-Sheet>.
- Muis, S., Haigh, I. D., Guimaraes Nobre, G. et al. (2018). Influence of El Niño-Southern Oscillation on Global Coastal Flooding. *Earth's Future*. DOI: [10.1029/2018ef000909](https://doi.org/10.1029/2018ef000909).
- Nascimento, J.L., Silvestre, M.R., and Neto, J.L.S. (2020). Trends and rainfall tropicalization in Paraná State, south of Brazil. *Atmosfera*, 33(1). DOI: [10.20937/atm.52441](https://doi.org/10.20937/atm.52441).
- Ouyang, Y., Zhang, J., Feng, G. et al. (2020). A century of precipitation trends in forest lands of the Lower Mississippi River Alluvial Valley. *Sci. Rep.*, 10, 12802. DOI: [10.1038/s41598-020-69508-8](https://doi.org/10.1038/s41598-020-69508-8).
- Petersen-Perlman, J.D., Aguilar-Barajas, I., and Megdal, Sh.B. (2022). Drought and groundwater management: Interconnections, challenges, and policy responses. *Current Opinion in Environmental Science and Health*, 28, 100364. DOI: [10.1016/j.coesh.2022.100364](https://doi.org/10.1016/j.coesh.2022.100364).
- Prange, M., Wilke, T., and Wesselingh, F.P. (2020). The other side of sea level change. *Commun. Earth Environ.*, 1, 69. DOI: [10.1038/s43247-020-00075-6](https://doi.org/10.1038/s43247-020-00075-6).
- Reigber, C., Lühr, H. and Schwintzer, P. (2002). CHAMP mission status. *Adv. Space Res.*, 30(2), 129–134. DOI: [10.1016/s0273-1177\(02\)00276-4](https://doi.org/10.1016/s0273-1177(02)00276-4).
- Ribes, A., Boe, J., Qasmi, S. et al. (2022). An updated assessment of past and future warming over France based on a regional observational constraint. *Earth Sys. Dyn.*, 13(4), 1397–1415. DOI: [10.5194/esd-13-1397-2022](https://doi.org/10.5194/esd-13-1397-2022).
- Ries, J., Bettadpur, S., Eanes, R. et al. (2016). The Combined Gravity Model GGM05C. GFZ Data Services. DOI: [10.5880/icgem.2016.002](https://doi.org/10.5880/icgem.2016.002).
- Rodell, M., Famiglietti, J.S., Wiese, D.N. et al. (2018). Emerging trends in global freshwater availability. *Nature*, 557, 651–659 (2018). DOI: [10.1038/s41586-018-0123-1](https://doi.org/10.1038/s41586-018-0123-1).
- Rummel, R. (2011). GOCE-the gravity steady-state ocean circulation explorer preface. *J. Geod.*, 85(11), 747. DOI: [10.1007/s00190-011-0499-2](https://doi.org/10.1007/s00190-011-0499-2).
- Sakumura, C. (2014). GRACE Technical Note 10 (CSR-GR-14-01) Gravity Recovery and Climate Experiment, Comparison of Degree 60 and Degree 96 Monthly Solutions, (May 5, 2014). Center for Space Research, The University of Texas at Austin.
- Sakumura, C., Bettadpur, S., and Bruinsma, S. (2014). Ensemble prediction and intercomparison analysis of GRACE time-variable gravity field models. *Geophys. Res. Lett.*, 41(5), 1389–1397. DOI: [10.1002/2013GL058632](https://doi.org/10.1002/2013GL058632).
- Sasgen, I., Martinec, Z., and Fleming, K. (2007) Wiener optimal combination and evaluation of the Gravity Recovery and Climate Experiment (GRACE) gravity fields over Antarctica. *J. Geophys. Res. Solid Earth*, 112, B04401. DOI: [10.1029/2006JB004605](https://doi.org/10.1029/2006JB004605).
- Save, H., Bettadpur, S., Tapley, B.D. (2016). High-resolution CSR GRACE RL05 mascons. *J. Geophys. Res. Solid Earth*, 121(10), 7547–7569. DOI: [10.1002/2016jb013007](https://doi.org/10.1002/2016jb013007).
- Save, H. (2019). GRACE Follow-On (CSR-GRFO-19-01 (GRACE-FO D-103920)) (Gravity Recovery and Climate Experiment Follow-On), CSR Level-2 Processing Standards Document (Rev. 1.1, June 06, 2019), (For Level-2 Product Release 06), Center for Space Research, The University of Texas at Austin.

- Schmied, H.M., Cáceres, D., Eisner, S. et al. (2021). The global water resources and use model WaterGAP v2.2d: model description and evaluation. *Geosci. Model Dev.*, 14(2), 1037–1079. DOI: [0.5194/gmd-14-1037-2021](https://doi.org/10.5194/gmd-14-1037-2021).
- Sun, Y., Riva, R., and Ditmar, P. (2016). Optimizing estimates of annual variations and trends in geocenter motion and J2 from a combination of GRACE data and geophysical models. *J. Geophys. Res. Solid Earth*, 121. DOI: [10.1002/2016JB013073](https://doi.org/10.1002/2016JB013073).
- Svehla, D. (2018). *Geometrical Theory of Satellite Orbits and Gravity Field*. Doctoral Thesis accepted by the Technische Universität München, Munich, Germany. Section 28.7. Temporal Variations in the Orientation of the Tri-Axial Earth's Ellipsoid and Low-Degree Sectorial Harmonics, 469–476.
- Tapley, B.D., Bettadpur, S., Watkins, M. et al. (2004). The gravity recovery and climate experiment: mission overview and early results. *Geophys. Res. Lett.*, 31, L09607. DOI: [10.1029/2004GL019920](https://doi.org/10.1029/2004GL019920).
- Tegel, W., Seim, A., Skiadaresis, G. et al. (2020). Higher groundwater levels in western Europe characterize warm periods in the Common Era. *Sci. Rep.*, 10, 16284. DOI: [10.1038/s41598-020-73383-8](https://doi.org/10.1038/s41598-020-73383-8).
- Wahr, J., Molenaar, M., and Bryan F. (1998). Time variability of the Earth's gravity field: Hydrological and oceanic effects and their possible detection using GRACE. *J. Geophys. Res.*, 103, 30205–30229. DOI: [10.1029/98JB02844](https://doi.org/10.1029/98JB02844).
- Watkins, M.M., Gruber, T., and Bettadpur, S. (2000). Science data system development plan. Tech. Rep. 327–710, GRACE Mission. Retrieved January 30, 2023, from [ftp://podaac.jpl.nasa.gov/allData/grace/docs/sds\\_dev\\_plan\\_c.pdf](ftp://podaac.jpl.nasa.gov/allData/grace/docs/sds_dev_plan_c.pdf).
- van Oldenborgh, G.J., Krikken, F., Lewis, S. et al. (2021). Attribution of the Australian bushfire risk to anthropogenic climate change. *Nat. Hazards Earth Syst. Sci.*, 21, 941–960. DOI: [10.5194/nhess-21-941-2021](https://doi.org/10.5194/nhess-21-941-2021).
- Yuan, D.-N. (2018). GRACE 327-744 (Gravity Recovery and Climate Experiment), JPL Level-2 Processing Standards Document, For Level-2 Product Release 06 (June 1, 2018), Jet Propulsion Laboratory, California Institute of Technology.
- Yuan, D.-N. (2019). GRACE Follow-On (JPL D-103921) (Gravity Recovery and Climate Experiment Follow-On), JPL Level-2 Processing Standards Document, For Level-2 Product Release 06 (May 28, 2019), Jet Propulsion Laboratory, California Institute of Technology.
- Yuan, S., Bao, F., Zhang, X. et al. (2022). Severe Biomass-Burning Aerosol Pollution during the 2019 Amazon Wildfire and Its Direct Radiative-Forcing Impact: A Space Perspective from MODIS Retrievals. *Remote Sens.*, 14(9), 2080. DOI: [10.3390/rs14092080](https://doi.org/10.3390/rs14092080).